



Harnessing Ag nanofilm as an electrons transfer mediator for enhanced visible light photocatalytic performance of Ag@AgCl/Ag nanofilm/ZIF-8 photocatalyst

Jianxin Liu, Rui Li, Yingyuan Hu, Tan Li, Zehui Jia, Yunfang Wang, Yawen Wang, Xiaochao Zhang, Caimei Fan*

College of Chemistry and Chemical Engineering, Taiyuan University of Technology, Taiyuan, Shanxi 030024, PR China

ARTICLE INFO

Article history:

Received 13 July 2016

Received in revised form 30 August 2016

Accepted 4 September 2016

Available online 5 September 2016

Keywords:

Ag nanofilm

Ag@AgCl/Ag nanofilm/ZIF-8

Ag@AgCl/ZIF-8

Electrons transfer mediator

Photocatalysis

ABSTRACT

An Ag@AgCl/Ag nanofilm/ZIF-8 composite photocatalyst was successfully constructed for the first time by loading Ag@AgCl and Ag nanofilm on the surface of ZIF-8 simultaneously via a simple deposition-photoreduction method. The formed Ag nanofilm was harnessed as a mediator to transfer photo-induced electrons from the plasmonic Ag@AgCl nanostructure to ZIF-8 for enhancing the photocatalytic reaction rate with visible light. The photocatalytic activity was evaluated by photocatalytic degradation of methylene blue (MB) under visible light irradiation. The first-order kinetic constant of MB degradation over Ag@AgCl/Ag nanofilm/ZIF-8 (14.762 h^{-1}) was nearly 2 times of Ag@AgCl/ZIF-8 (7.932 h^{-1}). The electrochemical impedance spectra, photoelectric conversion spectra and ESR DMPO- $\text{O}_2^{\bullet-}$ species spectra revealed that AFZ had a lower resistance, higher photocurrent density and more generation of superoxide radical than those of AZ, meaning that the extended interface between Ag nanofilm and ZIF-8 could promote the quick electrons transfer and electron-hole pairs separation. This work provides a new type electrons transfer mediator in fabrication of efficient plasmonic photocatalysts.

© 2016 Elsevier B.V. All rights reserved.

1. Introduction

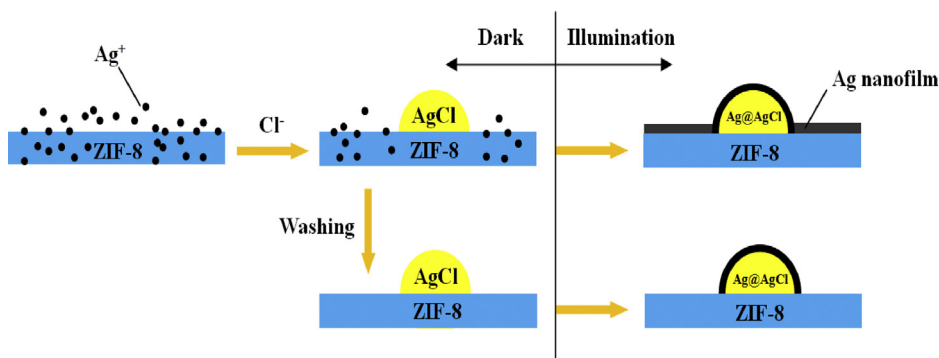
Semiconductor photocatalysis has been considered to be a promising green technology for solving the environmental pollution problems [1–4], and currently the main efforts are still focused on the development of highly efficient photocatalysts. Among various semiconductors, Ag@AgCl is one of the most effective catalysts and can be easily fabricated [5–9]. As early as 1990s, AgCl-based photocatalysts were reported to be efficient for the photocatalytic water splitting [10] and NO_x conversion [11]. In 2008, Huang and his colleagues first identified surface plasma resonance (SPR) Ag@AgCl photocatalyst, which aroused widespread attention due to its highly efficient and stable photocatalytic activity under visible light [12]. SPR effect improve the photocatalytic activity of photocatalyst by extending light absorption to longer wavelengths and transferring the plasmonic electrons from the SPR metal to the conduction band (CB) of semiconductor [13–15].

However, the photoactivity of Ag@AgCl is limited by the poor reducing capacity of AgCl with relatively lower CB potential, which is not conducive to the utilization of photon-induced electrons. Then coupling another strong reducing photocatalyst (SP2), which has a relatively higher CB potential, in Ag@AgCl to provide the utilization of photon-induced electrons should be an effective way to solve this problem. Several strong reducing photocatalysts with high CB potential, such as La(OH)₃ [16], TaON [17], NaTaO₃ [18], have been applied to improve the photocatalytic activity of Ag@AgCl. Due to the high reducing capacity of SP2, the SPR electrons can be transferred from SPR metallic Ag to SP2 and combined with O₂ to form O₂ $^{\bullet-}$, which is a main active species for photocatalytic degradation reactions [16,19,20]. This means that building an Ag@AgCl/SP2 composite photocatalyst system with matching band structures is feasible for improving the effective reaction of electrons and the photodegradation performance of organics. Then transfer more electrons from SPR metallic Ag to the CB of the SP2 is the key to further enhance the photocatalytic activity of Ag@AgCl/SP2 composite photocatalyst system.

Usually, using metal nanostructure as a conductive medium is a powerful method for the enhanced transformation of photoinduced charges [21]. For example, noble metal Ag, due to the

* Corresponding author.

E-mail address: fancm@163.com (C. Fan).



Scheme 1. Illustration of the preparation process of AZ and AFZ.

electrons storage and discharge properties, had always been used as an electronic mediator in hybrid photocatalysis [22–25]. The contact interface area between noble metal mediator and photocatalyst is another crucial factor in ensuring a fast continuous flow of electrons [26–29]. With spatial analytic geometry, paving noble metal nanofilm on the surface of photocatalyst should be an ideal solution to achieve surface-to-surface contact between mediator and photocatalyst, which can effectively improve the electrons transfer. Unfortunately, noble metal nanofilm technology has not been reported in the photocatalytic fields so far, and most synthetic methods of metal nanofilms need complex synthetic procedures or additives [30–32]. Therefore, a simple synthetic method for loading noble metal nanofilm on the surface of photocatalysts is an urgent necessity.

Herein, we designedly fabricated a novel Ag@AgCl/Ag nanofilm/ZIF-8 composite photocatalyst by loading Ag@AgCl and Ag nanofilm on the surface of ZIF-8 simultaneously via a simple deposition-photoreduction method without any additives. ZIF-8 is constructed from Zn²⁺ and imidazolate organic ligands center ions [33–36], which exhibits higher thermal and chemical stability than other MOFs [37–40]. Due to the strong reducing capacity, ZIF-8 was acted as SP2. The formed Ag nanofilm was harnessed as a mediator to transfer photo-induced electrons from the plasmonic Ag@AgCl nanostructure to ZIF-8. Compared with Ag@AgCl/ZIF-8 (AZ), the Ag@AgCl/Ag nanofilm/ZIF-8 (AFZ) photocatalytic system showed obviously enhanced photocatalytic activity for the photodegradation of MB in solution. In order to explore the actual role of Ag nanofilm in the visible photocatalytic process, the as-synthesized AFZ and AZ were investigated by electrochemical impedance, photocurrent and electron spin resonance (ESR). According to the systematic analysis, a photocatalytic mechanism of AFZ photocatalytic system has been proposed. To our best knowledge, this is the first report that using Ag nanofilm as an electrons mediator to enhance visible light photocatalytic performance of composite photocatalyst.

2. Experimental

2.1. Materials

Ammonia solution, methanol, and silver nitrate were purchased from Sinopharm. Zinc chloride and 2-methylimidazole were purchased from Aladdin. All reagents were of analytical grade purity and used without further purification.

2.2. Preparation of photocatalysts

Preparation of ZIF-8

ZIF-8 nanocrystals were prepared following the procedures previously reported [41]. Typically, 0.78 g of Zn(OH)₂ and 1.298 g of

2-methylimidazole (Hmim) were dissolved in 100 mL of aqueous ammonia (28%) and 20 mL of methanol (MeOH) separately, and then the Hmim solution was poured into the Zn(OH)₂ solution under magnetic stirring. The mixture was stirred at room temperature. After 2 days, the solid product was separated from the milky colloidal dispersion by centrifugation and washed three times with 100 mL of H₂O/MeOH (1:1 v/v) mixture.

Preparation of Ag nanofilm/ZIF-8

The ZIF-8 (0.1 g) was immersed into a solution of silver nitrate (0.05 M) under vigorous stirring and was irradiated by UV-vis light for 30 min. Then a precipitate was separated from the solution by vacuum filtration, washed with deionized water, and dried in the air at 60 °C for 2 h.

Preparation of Ag@AgCl

Typically, 1 mmol of ZnCl₂ was added to 44 mL of AgNO₃ solution (0.05 M) under vigorous stirring. After 30 min, the obtained white suspension was reduced by UV-vis light for 30 min under stirring. A black precipitate appeared and was separated from the solution by vacuum filtration, washed with deionized water, and dried in the air at 60 °C for 2 h.

2.3. Preparation of AFZ and AZ

The preparation process of AFZ and AZ were represented schematically in Scheme 1. In a typical synthesis, 0.1 g of ZIF-8 was added to 44 mL of AgNO₃ aqueous solution (0.05 M) under stirring. After the addition, the mixed suspension was kept vigorously stirring for 30 min to ensure ZIF-8 was evenly dispersed in solution. Then 1 mmol of ZnCl₂ was added to the suspending solution, and the mixture was kept stirring for 30 min. Because the Ag⁺ was overdose compared with Cl⁻, part of the Ag⁺ reacted with the Cl⁻ to form AgCl nano-particles (NPs) and loaded on the surface of the ZIF-8, while the residual Ag⁺ still stayed in solution. Next, the above suspension was irradiated by UV-vis light for 30 min under stirring. Metallic Ag was appeared on the surface of AgCl and ZIF-8 simultaneously due to the photo-reduction. The theoretical weight fraction of Ag nanofilm in AFZ composition was 5 wt%. The other samples of AFZ with 2, 10, 20 wt% of Ag nanofilm were also synthesized following the same procedure by only adjusting the amount of AgNO₃. For comparison, AZ was prepared under same conditions but the residual Ag⁺ was washing out using distilled water before the photoreduction process.

2.4. Characterization

The crystalline phases of the samples were examined by an X-ray diffraction (XRD) instrument (Rigaku, D/max-2500) using Cu K α radiation ($\lambda = 0.15406$ nm) within the 2θ range of 10° to 80°. The accelerating voltage and applied current were 40 kV and 30 mA,

respectively, and the scan rate was 8° min^{-1} . X-ray photoelectron spectroscopy (XPS) measurements were performed on a Thermo ESCALAB 250 Xi XPS system with an Al Ka ($\text{hv} = 1486.6 \text{ eV}$) 150 W, 500 μm beam spot source. The shift in binding energy caused by relative surface charges was referenced to the C 1s peak of the surface adventitious carbon. Transmission electron microscopy (TEM) images were obtained by a JEOL JEM-2010 (HT) instrument at the accelerating voltage of 200 kV. In situ electron spin resonance (ESR) spectra were conducted on a Bruker model ESR JES-FA200 spectrometer. The Brunauer–Emmett–Teller (BET) surface areas were measured by nitrogen adsorption isotherm measurements at 77 K on a JW-BK instrument. The scanning electron microscope (SEM) images were recorded on a Nanosem 430 Field Emission Scanning Electron Microscope. Atomic force microscopy (AFM) images were taken in tapping mode on a multimode nanoscope IIIa controller (Veeco, USA). Fourier transform infrared (FT-IR) spectra were recorded on a Shimadzu-8400S spectrometer in the range of 400–4000 cm^{-1} using KBr pellets. The light absorption properties of the samples were recorded on an ultraviolet-visible (UV-vis) spectrophotometer. Silver and zinc in the water were measured by an inductively coupled plasma atomic emission spectrometer (Leeman, PROFILE SPEC). TOC was determined with a total organic carbon analyser (Elementar, Germany).

2.5. Photocatalytic activity

The photocatalytic activities of the as-synthesized samples were investigated by the photocatalytic degradation of MB in aqueous solution under visible light irradiation. The photochemical reactor was illuminated by a 500 W xenon lamp with a 420 nm cut off filter. The distance between the light and the centre of the reactor was 20 cm. The intensity of light (120.2 klx) was measured by a digital light meter. In each test, 100 mg of as-synthesized samples were added into 100 mL of 10 mg L^{-1} MB aqueous solution. Then the suspension was stirred in the dark for 20 min to achieve the adsorption–desorption equilibrium prior to visible light irradiation. At given time interval, 5 mL of the suspension was taken out and centrifuged. The supernatant solution was analyzed by a Varian Cary-50 UV-vis spectrophotometer. The apparent pseudo-first-order model expressed by following equation is employed:

$$\ln(C_0/C) = kt + \ln(C_0/C_1)$$

where k is the pseudo-first-order rate constant, C_0 is the initial concentration of MB, C_1 is the concentration of MB after adsorption, and C is the concentration of MB at reaction time t .

2.6. Photoelectrochemical measurements

The photocurrents (PC) electrochemical, impedance spectroscopy (EIS) and Mott–Sckottky measurements were performed by an electrochemical analyzer (Solartron SI 1287 Instruments) in a three-electrode quartz cell with Na_2SO_4 (0.1 M) solution. The as-synthesized samples of AFZ and AZ were deposited on a fluorinated-tin-oxide (FTO) conducting glass ($0.5 \times 5 \text{ cm}$) as the working electrode. Calomel electrode was used as the reference electrode, and Pt worked as the counter electrode. A 500 W Xenon lamp served as UV-vis light source.

2.7. Silver and zinc release from the AZ and AFZ

Six parallel tests were conducted to test silver and zinc release. For each test, 0.1 g AZ or AFZ nanocomposite was immersed in a flask containing 10 mL distilled water at room temperature under stirring. At given time intervals (1, 2, 3, 5, 7, 10 days), the concentra-

tions of Ag and Zn were measured by inductively coupled plasma analysis (ICP), which was used previously by other researchers [42].

3. Results and discussion

3.1. Characterization of the photocatalysts

The morphologies of as-synthesized samples were examined by TEM. The pure ZIF-8 sample consists of sheet-shaped structures with a smooth surface (Fig. 1a). Fig. 1b shows the morphology of Ag nanofilm/ZIF-8, indicating that the surface of ZIF-8 is coated by a film-like substance and shows a much rougher surface than that of ZIF-8. The high-resolution TEM (HRTEM) image of Ag nanofilm/ZIF-8 (Fig. 1c) confirms that the film-like substance is comprised by a large amount of Ag small nanoparticles (NPs) enclosed by Ag (111). It would be likely that ZIF-8 provides numerous nucleation sites for the growth of Ag nanoparticles, leading to homogeneous dispersion of Ag nanoparticles on the ZIF-8 with a smaller size. AZ (Fig. 1d) and AFZ (Fig. 1f) show a similar structure that the well-defined Ag@AgCl NPs (20–50 nm) are loaded on the surface of a sheet structure support. Interestingly, the enlarged TEM image of AZ (inset in Fig. 1d) shows that the ZIF-8 in AZ remains a smooth surface, while the ZIF-8 in AFZ (inset in Fig. 1f) is covered by Ag nanofilm and shows a rough surface. These observations clearly indicated that Ag nanofilm is coated on the surface of ZIF-8, and the extended interface between Ag nanofilm and ZIF-8 may promote the electron-hole pairs separation.

The element distribution and composition of AZ and AFZ were subsequently analyzed by EDX spectroscopy. EDX maps of the composites and the elements of C, N, Zn, Ag and Cl are presented in Fig. 2. Both for AZ and AFZ, Zn, C, and N are distributed uniformly, which indicates a good dispersion of each element in ZIF-8, and the Cl element is scattered on the entire area due to the AgCl was decomposed by electronic beam during the EDX test. The local relative concentration of each element presented in the sample is indicated by the relative brightness and the intensity of the color. For the Ag elements in AZ, the EDX map shows that the silver elements gathered in the Ag@AgCl sites. However, for the Ag elements in AFZ, the homogeneous low density blue nightspots are uniformly distributed at or in the whole test area except the dense blue nightspots corresponded to the Ag@AgCl NPs, which further confirms the existence of the Ag nanofilm on the surface of ZIF-8. To evaluate the thickness of the Ag nanofilm, AFM measurement was carried out as shown in Fig. 3. The AFM result reveals that the thickness of the Ag nanofilm/ZIF-8 and Ag nanofilm are approximately 20 nm and 5 nm, respectively.

The phase structures of the as-synthesized samples were confirmed by XRD analysis (Fig. 4). Almost all of the XRD peaks for ZIF-8 were in good agreement with previous report [43], confirming the formation of pure crystalline ZIF-8 phase. In the XRD spectrum of Ag/AgCl, the diffraction peaks at 27.8° , 32.2° , 46.2° , 54.8° and 57.5° are attributed to (111), (200), (220), (311) and (222) crystal planes of AgCl (JCPDS No. 85-1355) and the weak peaks appeared around the scattering angle of 38.1° can be ascribed to the metallic Ag (JCPDS No. 87-717). Both of AZ and AFZ composites exhibit a coexistence of AgCl, ZIF-8 and metallic Ag without any impurity phase. These indicate that the framework of ZIF-8 was stable throughout the entire process of catalyst preparation. It's worth noting that the agreement of AFZ composite photocatalyst patterns with those of AZ indicates the introduction of Ag nanofilm do not change the crystal phase and crystallinity of AZ. Moreover, the AZ and AFZ also exhibit similar FTIR spectra (Fig. S1), and analogous morphology in the SEM images (Fig. S2).

The elemental composition and chemical status of the as-prepared samples were examined by X-ray photoelectron spec-

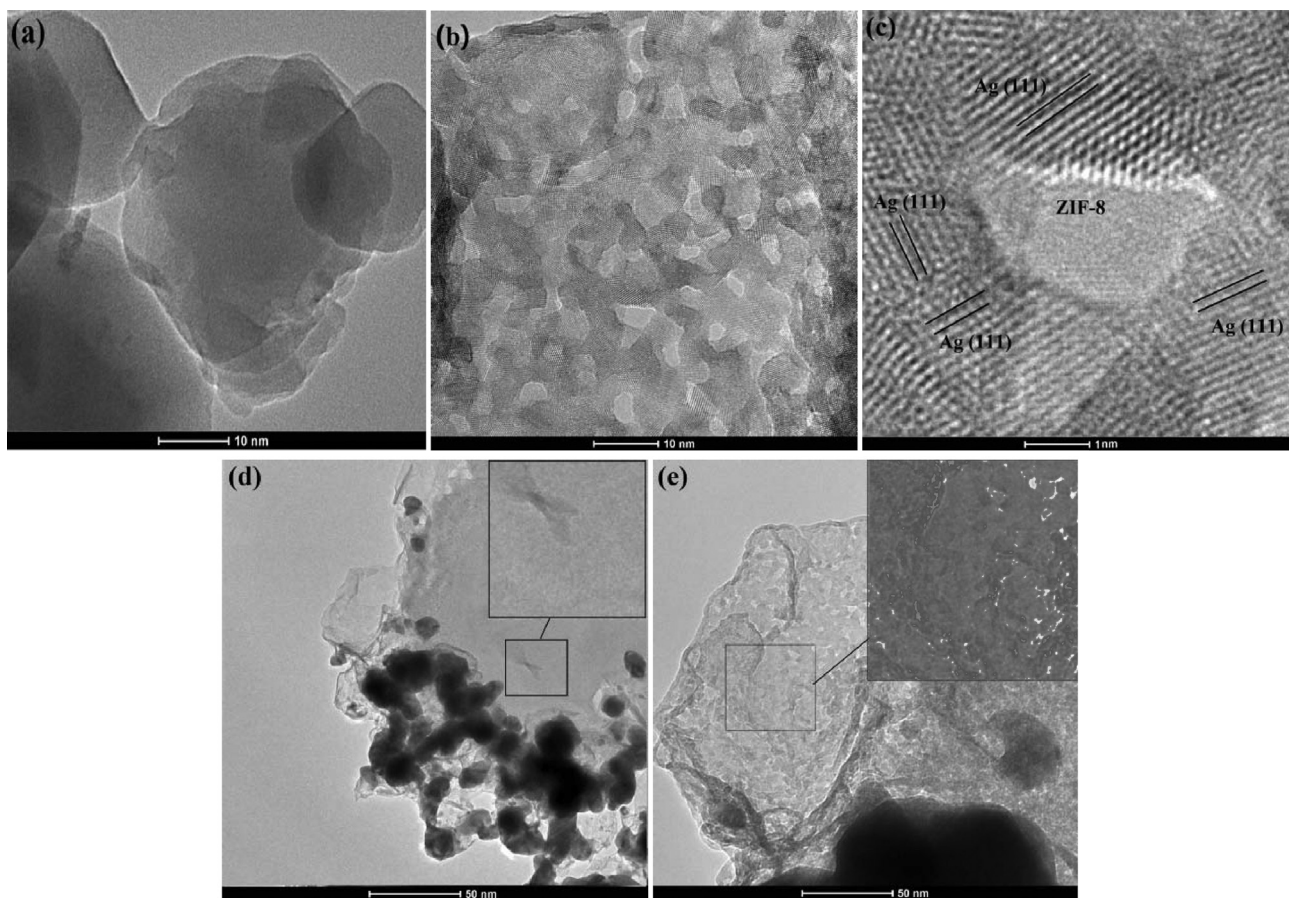


Fig. 1. TEM images of (a) ZIF-8, (b) Ag nanofilm/ZIF-8, (c) HRTEM images of Ag nanofilm/ZIF-8, (d) AZ and (e) AFZ.

troscopy (XPS). Fig. 5 shows the X-ray photoelectron spectroscopy (XPS) narrow scan of the Ag region in AZ and AFZ, where two main components of the Ag 3d envelope are shown in each panel. This analysis also reveals that the relative content of Ag^0 in AFZ is higher than that of AZ, which supports that the Ag nanofilm is comprised of metallic Ag. AZ and AFZ show same Zn 2p, O 1s, N 1s, and Cl 1s XPS spectra, which have been provided and discussed in Supporting information (Fig. S3)[37,43]. These indicate that the formed Ag nanofilm in AFZ did not affect the presence of Zn, N, O, and Cl element.

The sample of bare ZIF-8 attains a large surface area (S_{BET}) of $1627.28 \text{ m}^2 \text{ g}^{-1}$ (Fig. 6). After deposited Ag@AgCl, the BET surface area of ZIF-8 decreases to $576.10 \text{ m}^2 \text{ g}^{-1}$, but it is still much larger than that of Ag@AgCl ($4.62 \text{ m}^2 \text{ g}^{-1}$). These results demonstrate that AZ still maintains the relatively larger surface area and porous structure of ZIF-8. However, when Ag@AgCl and Ag nanofilm are loaded on the surface of ZIF-8 simultaneously, the BET surface area of the AFZ is only $22.8577 \text{ m}^2 \text{ g}^{-1}$. This obvious decrease of BET surface area further confirms that the surface of ZIF-8 is almost wholly covered by Ag nanofilm.

The optical absorption of AZ and AFZ was measured using a UV-vis diffuse reflectance spectrometer. The same absorbance ranges between AZ and AFZ are found (Fig. S4). It is known that the AgCl and ZIF-8 cannot be excited by visible light. The observed band in the region 400–1000 nm can be attributed to the typical SPR effect of metallic Ag. The SPR absorb intensity of AFZ is slightly weaker than AZ, which may attribute to the different morphology and/or local dielectric environment of metallic Ag.

The Ag and Zn release from the AZ and AFZ nanocomposites were also investigated. In order to better understand the mass

loss of silver element during the soaking process, $\text{Ag}_{\text{release}}/\text{Ag}_0$ and $\text{Zn}_{\text{release}}/\text{Zn}_0$ were used to describe the silver and zinc release performance, where $\text{Ag}_{\text{release}}(\text{Zn}_{\text{release}})$ is the mass of silver(zinc) element released in water and $\text{Ag}_0(\text{Zn}_0)$ is the mass of the original silver(zinc) element in photocatalysts. Fig. 7a shows the amount of the released silver element in water as a function of soaking time at room temperature. In the first five days silver is highly released for both AZ and AFZ nanocomposites, after that, the silver ion releasing rate is changed slower. The amount of the released silver for AFZ nanocomposite is higher than that of AZ, which may attribute to the extended interfacial area between Ag nanofilm and the solution. After 10 days soaking process, the silver element mass losses of AZ and AFZ are 5.32% and 5.95%, respectively. Fig. 7b shows the zinc element released curves of AZ and AFZ in water. It is noteworthy that, after 10 days soaking process, the zinc element mass losses of AFZ is 7.90%, while zinc release from AZ is 9.41%, this means that the Ag nanofilm covered on the surface of ZIF-8 can avoid the zinc element released from the AFZ at some extent.

3.2. Photocatalytic activity

Fig. 8 shows the photocatalytic activity of the as-synthesized samples for the MB removal from the water under visible light irradiation ($\lambda > 420 \text{ nm}$). The blank test confirms that MB is only slightly degraded under visible light irradiation in the absence of catalyst, indicating that the photolytic effect can be ignored. It is obvious that MB is degraded faster in the presence of AFZ and AZ composite photocatalysts than in the presence of the Ag@AgCl photocatalyst. Furthermore, the apparent reaction rate constant (k) of AFZ (14.762 h^{-1}) is almost double of AZ (7.932 h^{-1}), which indicates that the photocatalytic activity of AFZ is significantly higher than that of AZ.

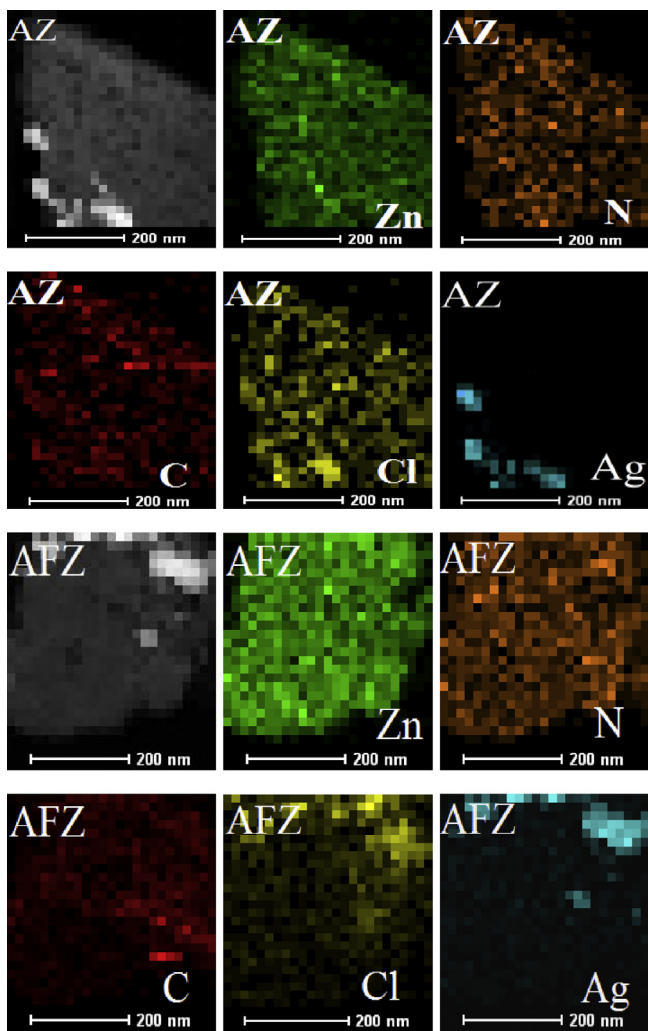


Fig. 2. TEM energy-dispersive X-ray (TEM-EDX) mappings of AZ and AFZ.

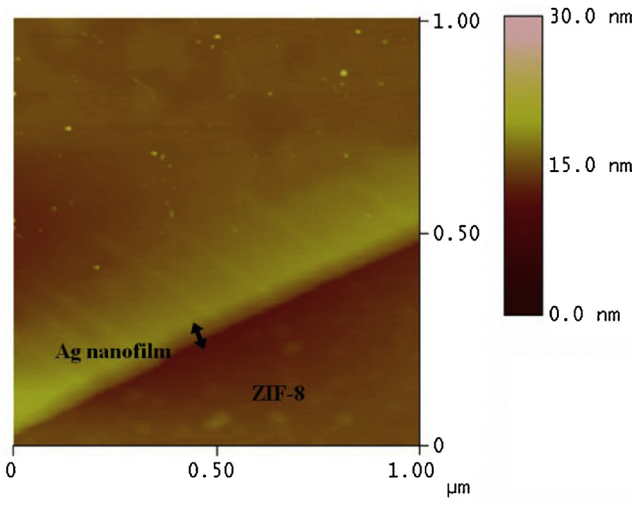


Fig. 3. AFM image of AFZ.

ing that the presence of Ag nanofilm can effectively promote the photocatalytic activity. The influence of different amounts of Ag nanofilm on photocatalytic activity is also studied (Fig. S5), when 5 wt% Ag nanofilm is introduced, the AFZ shows the best activity among all the composites. It can be noted that ZIF-8 (5.06 eV,

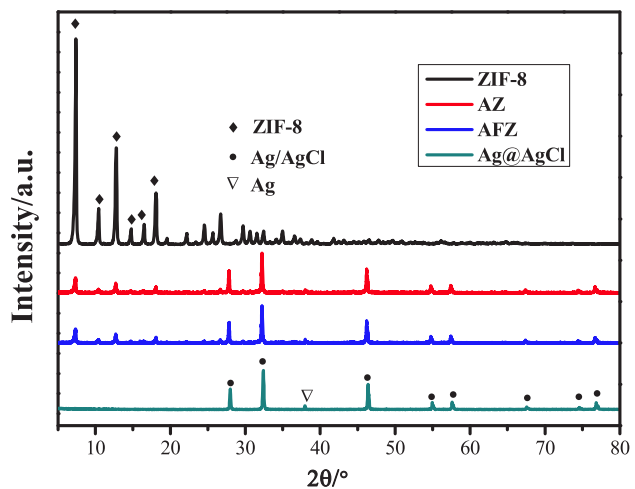


Fig. 4. XRD patterns of ZIF-8, AZ, AFZ and Ag@AgCl.

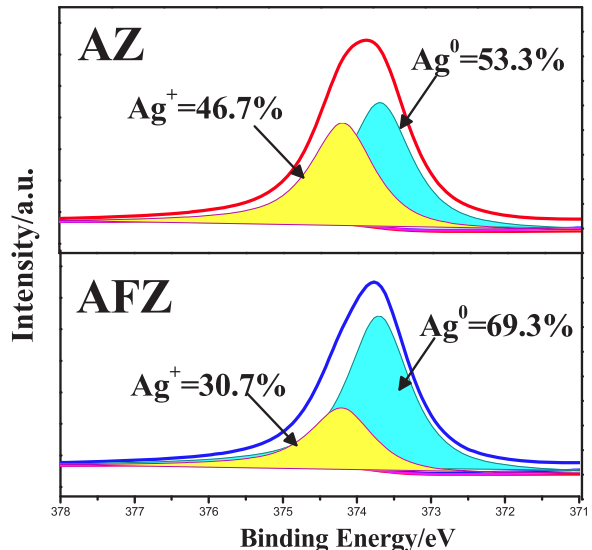


Fig. 5. The Ag 3d XPS spectra of AZ and AFZ.

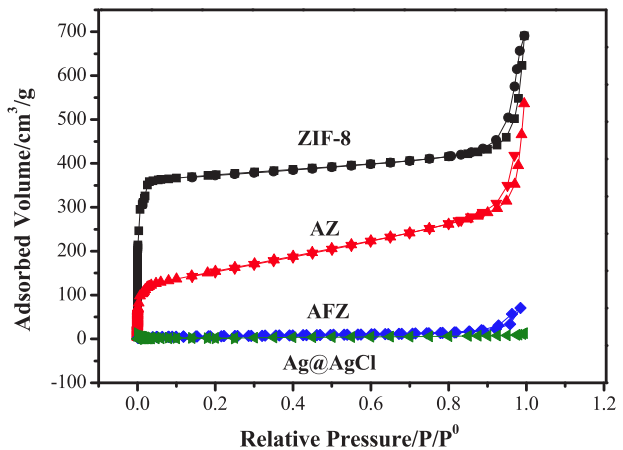


Fig. 6. N₂ adsorption–desorption isotherms of ZIF-8, AZ, AFZ and Ag@AgCl.

Fig. S6a) and AgCl (3.25 eV) [13] cannot be excited by visible light. The Ag@AgCl composites show some visible-light-driven photocatalytic activity, while Ag nanofilm/ZIF-8 is visible photocatalytic activity inertia. These mean that only the metallic Ag on the sur-

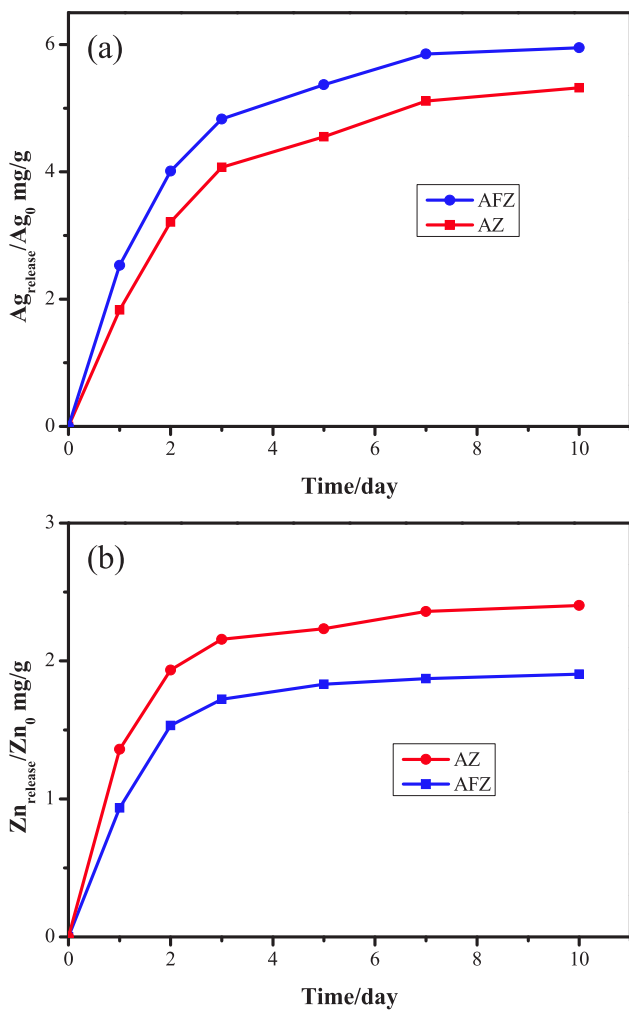


Fig. 7. The silver (a) and zinc (b) release curve of the AZ and AFZ.

face of AgCl works as a photosensitizer for SPR effect, while the Ag nanofilm on the surface of ZIF-8 cannot absorb visible light, because the SPR effect largely depends on the surrounding environment of noble metal [14].

The mineralization efficiency was calculated from total organic carbon (TOC) measurements (Fig. S7). It was found that the as-prepared AFZ hybrid hydrogels exhibited higher performance in TOC removal of MB solution than that of AZ. After 12 min visible light illumination, the TOC removal by AZ and AFZ were 42.25% and 53.39%, respectively. This further illustrated that the formed Ag nanofilm plays an important role in the electrons transfer for the photocatalytic degradation of MB.

Fig. S8 shows that the as-synthesized AZ and AFZ maintain a relative high photocatalytic activity for the removal of MB dyes during all five cycles, which may attribute to the effective electron transfer and the trace silver/zinc releasing. The crystal structures of the AZ and AFZ after double repeated photocatalytic reaction are exhibited in Fig. S9. There are no significant differences between the fresh and used samples, indicating that the AZ and AFZ have good stability during the photodegradation of MB.

3.3. Photocatalytic mechanism

The photocatalyst efficiency is mainly decided by the following three important aspects: (1) photoinduced charges generation, that is, how to sufficiently absorb photons in the solar energy spectrum; (2) photoinduced charges separation, that is, how to

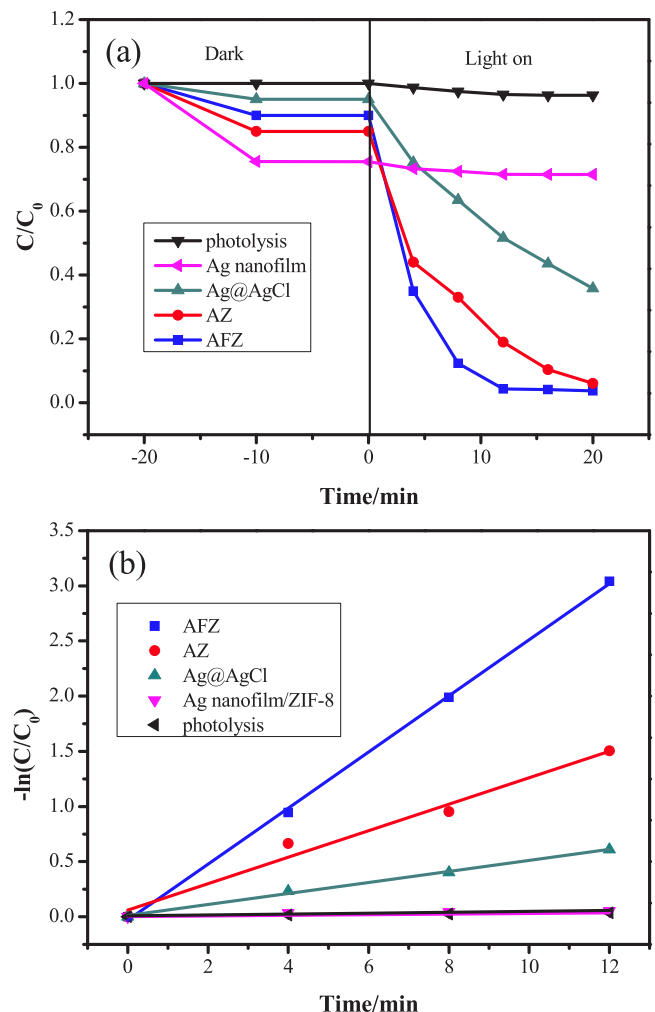


Fig. 8. Time-course variation of (a) C/C₀ of MB solution and (b) Pseudo-first order kinetics for the degradation of MB.

effectively avoid the recombination of excitons; (3) photoinduced charges utilization, that is, how to maximally utilize the excitons to drive redox reaction [27,44,45]. Based on the DRS spectra, the photon absorption efficiency of AFZ is slightly weaker than AZ, and then the photocatalytic activity enhancement should come from the improved photoinduced charges separation and/or utilization. For proving this point, the electrochemical impedance of AFZ and AZ was conducted as showed in Fig. 9. The AFZ displays smaller diameter of the Nyquist circle than AZ, revealing the lower interfacial charge-transfer resistance of AFZ. The separation efficiency of electron–hole pairs of AZ and AFZ was also investigated by photoelectric current experiments and demonstrated in Fig. 10. Both samples show a quick response to the light but it could be found that the photocurrent over AFZ is higher than that of AZ, which suggested that AFZ had a more efficient separation for the photogenerated electron–hole pairs. These results of photocurrent density and electrochemical impedance clarify that it is the Ag nanofilm in AFZ sample plays important role, and hence led to the strikingly lower resistance and higher photoinduced charges separation of AFZ.

The separated charges can react with H₂O or O₂ to form reactive oxygen species (ROS), which as the main active species are responsible for photocatalytic reaction [20,46]. An examination of the ROS formation can provide useful information for the fate of the photoinduced electrons and further lead to a greater understanding of the electrons utilization. Therefore, the ESR spin-trap tests with 5,5-

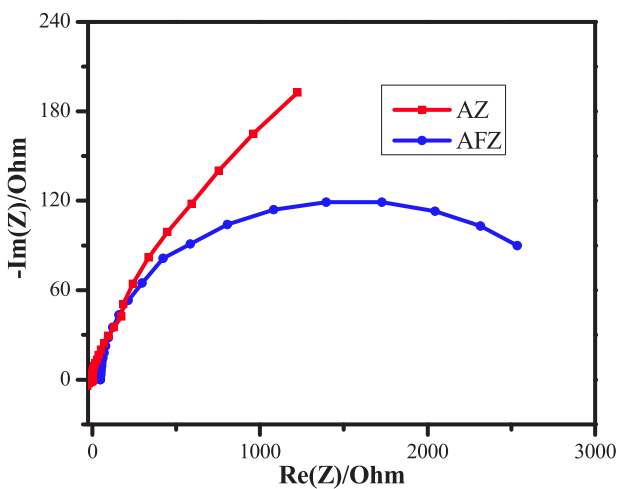


Fig. 9. Electrochemical impedance spectra of AZ and AFZ.

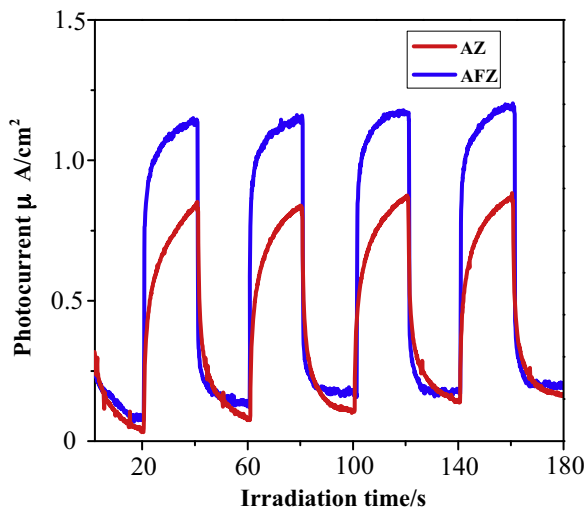


Fig. 10. Photoelectric conversion performances of AZ and AFZ in 0.1 M Na₂SO₄ aqueous solutions and under visible light irradiation ($\lambda > 420$ nm).

dimethyl-1-pyrroline N-oxide (DMPO) were performed, and the result is displayed in Fig. 11. No ESR signals are detected when the reaction is carried out in the dark for both AZ and AFZ. Under visible light irradiation (450 nm), characteristic peaks from the DMPO-O₂^{•-} species can be observed in both AZ and AFZ, and the peak intensity of AFZ in the DMPO-O₂^{•-} species is relatively stronger than that of AZ. This result demonstrates that the Ag nanofilm in AFZ can effectively promote the utilization of electrons.

Based on the above data, a photocatalytic mechanism of AFZ photocatalyst was proposed in Scheme 2. It is obvious that ZIF-8 (5.06 eV) and AgCl (3.25 eV) cannot be excited by visible light. Due to the existence of SPR metallic Ag (on AgCl), the visible light can be absorbed by the photocatalyst, and the absorbed photon will be changed into electrons and holes (Scheme 2a). The holes transfer to the AgCl surface, which corresponds to the oxidation of Cl⁻ ions to Cl[•] radicals, then Cl[•] oxidizes MB and are reduced to Cl⁻ ions again. As for the electrons, there are two possible pathways for the transfer and utilization that the photoinduced electrons are transferred from SPR metallic Ag to the CB of AgCl or ZIF-8. The CB position of AgCl (-0.09 eV vs NHE) is very close to the E₀(O₂/O₂^{•-}) (-0.046 eV vs NHE) [13], which leads to an unfavorable driving-force for the generation of O₂^{•-} due to the presence of the overpotential [47]. The CB position of AgCl (-0.09 eV vs NHE) is very close to the E₀(O₂/O₂^{•-})

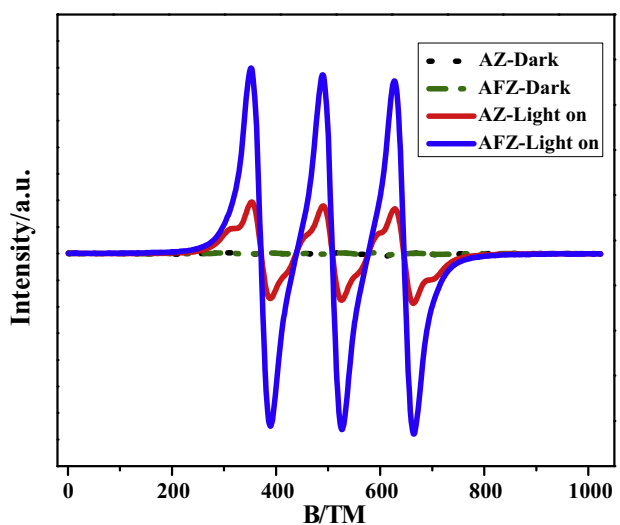
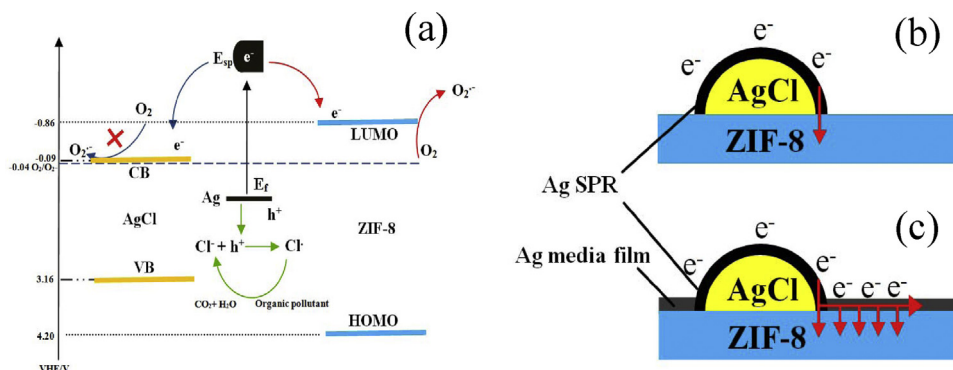


Fig. 11. ESR DMPO-O₂^{•-} species spectra of AZ and AFZ under visible light irradiation.

(-0.046 eV vs NHE), which leads to an unfavorable driving-force for the generation of O₂^{•-} due to the presence of the overpotential [47]. The CB position of ZIF-8 (-0.86 eV vs NHE; see Supporting information) is distinctly more negative than that of E₀(O₂/O₂^{•-}), indicating that ZIF-8 in composite photocatalyst is beneficial to the generation of O₂^{•-} [48–51]. Therefore the precise role of ZIF-8 in the AFZ is molecular oxygen activation. It can be concluded that the injection of the SPR electrons into the CB (LUMO) of ZIF-8 is profitable to the photocatalytic performance of this photocatalytic system. This is why the AZ shows a higher photocatalytic activity than that of Ag@AgCl. However, this electrons transfer is limited by the poor interface area between SPR metallic Ag and ZIF-8, as show in Scheme 2b. But for the AFZ photocatalytic system, the Ag nanofilm cover the surface of ZIF-8 and work as an electronic mediator to connect SPR metallic Ag and ZIF-8, the broadening contact interface area between Ag nanofilm and ZIF-8 provides extensive channels for the electrons transfer from SPR metallic Ag to ZIF-8 (Scheme 2c), as a result, the photoinduced electrons in AFZ photocatalytic system are not only effectively separated, but also utilized to generate more O₂^{•-}. That is metallic silver in different location of the AFZ photocatalytic system plays different roles. The metallic silver on the surface of AgCl acts as the SPR metal for light-harvesting, while on the surface of ZIF-8 works as electronic medium for enhancing the photoinduced electrons separation and utilization.

4. Conclusions

In summary, a novel Ag@AgCl/Ag nanofilm/ZIF-8 (AFZ) composite photocatalyst with an extended direct contact between Ag nanofilm and ZIF-8 has been successfully developed for the first time via a precipitation-photoreduction method and demonstrated an enhanced visible light photocatalytic activity for MB decomposition compared with Ag@AgCl/ZIF-8 (AZ) photocatalyst. Moreover, the reduced resistance, improved photocurrent and increased superoxide radical generation are observed and proved that the Ag nanofilm in AFZ could accelerate the separation and utilization of photoinduced charges. A reasonable mechanism for the enhanced photoactivity is proposed by harnessing Ag nanofilm as a mediator to promote the electrons transfer from the SPR metallic Ag to ZIF-8 with strong reducibility. The present study provides a new conception in construction of high performance plasmonic photocatalysts with improved electrons transfer for environmental remediation.



Scheme 2. (a) Possible photocatalytic reaction mechanism of MB over AFZ under visible light irradiation; Scheme of electron transfer from plasmonic metal to ZIF-8 (b) AZ and (c) AFZ.

Acknowledgement

This work was financially supported by the Youth National Natural Science Foundation of China (No. 21206105, No. 21506144) and the National Natural Science Foundation of China (No. 21176168).

Appendix A. Supplementary data

Supplementary data associated with this article can be found, in the online version, at <http://dx.doi.org/10.1016/j.apcatb.2016.09.015>.

References

- [1] J. Tian, Z. Zhao, A. Kumar, R.I. Boughton, H. Liu, Chem. Soc. Rev. 43 (2014) 6920–6937.
- [2] Y. Qu, X. Duan, Chem. Soc. Rev. 42 (2013) 2568–2580.
- [3] T. Hisatomi, J. Kubota, K. Domen, Chem. Soc. Rev. 43 (2014) 7520–7535.
- [4] W. Wang, M.O. Tade, Z. Shao, Chem. Soc. Rev. 44 (2015) 5371–5408.
- [5] C. An, S. Wang, Y. Sun, Q. Zhang, J. Zhang, C. Wang, J. Fang, J. Mater. Chem. A 4 (2016) 4336–4352.
- [6] S. Zhang, J. Li, X. Wang, Y. Huang, M. Zeng, J. Xu, ACS Appl. Mater. Interfaces 6 (2014) 22116–22125.
- [7] Y. Fan, W. Ma, D. Han, S. Gan, X. Dong, L. Niu, Adv. Mater. 27 (2015) 3767–3773.
- [8] X. Li, S. Fang, L. Ge, C. Han, P. Qiu, W. Liu, Appl. Catal. B 176–177 (2015) 62–69.
- [9] C. Han, L. Ge, C. Chen, Y. Li, Z. Zhao, X. Xiao, Z. Li, J. Zhang, J. Mater. Chem. A 2 (2014) 12594.
- [10] M. Lanz, G. Calzaferri, J. Photochem. Photobiol. A 109 (1997) 87–89.
- [11] Y. Yamashita, N. Aoyama, N. Takezawa, K. Yoshida, J. Mol. Catal. A 150 (1999) 233–239.
- [12] P. Wang, B. Huang, X. Qin, X. Zhang, Y. Dai, J. Wei, M.H. Whangbo, Angew. Chem. Int. Ed. 47 (2008) 7931–7933.
- [13] L. Ye, J. Liu, C. Gong, L. Tian, T. Peng, L. Zan, ACS Catal. 2 (2012) 1677–1683.
- [14] W. Hou, S.B. Cronin, Adv. Funct. Mater. 23 (2013) 1612–1619.
- [15] R. Jiang, B. Li, C. Fang, J. Wang, Adv. Mater. 26 (2014) 5274–5309.
- [16] X. Xiao, W. Zhang, J. Yu, Y. Sun, Y. Zhang, F. Dong, Catal. Sci. Technol. 6 (2016) 503–510.
- [17] J. Hou, C. Yang, Z. Wang, Q. Ji, Y. Li, G. Huang, S. Jiao, H. Zhu, Appl. Catal. B 142–143 (2013) 579–589.
- [18] D. Xu, W. Shi, C. Song, M. Chen, S. Yang, W. Fan, B. Chen, Appl. Catal. B 191 (2016) 228–234.
- [19] W. He, H.K. Kim, W.G. Wamer, D. Melka, J.H. Callahan, J.J. Yin, J. Am. Chem. Soc. 136 (2014) 750–757.
- [20] H. Jia, W. He, W.G. Wamer, X. Han, B. Zhang, S. Zhang, Z. Zheng, Y. Xiang, J.J. Yin, J. Phys. Chem. C 118 (2014) 21447–21456.
- [21] H. Tada, T. Mitsui, T. Kiyonaga, T. Akita, K. Tanaka, Nat. Mater. 5 (2006) 782–786.
- [22] Y. Yang, W. Guo, Y. Guo, Y. Zhao, X. Yuan, Y. Guo, J. Hazard. Mater. 271 (2014) 150–159.
- [23] Y. Chai, J. Ding, L. Wang, Q. Liu, J. Ren, W.-L. Dai, Appl. Catal. B 179 (2015) 29–36.
- [24] F. Chen, Q. Yang, X. Li, G. Zeng, D. Wang, C. Niu, J. Zhao, H. An, T. Xie, Y. Deng, Appl. Catal. B 200 (2017) 330–342.
- [25] H. Li, H. Yu, X. Quan, S. Chen, Y. Zhang, ACS Appl. Mater. Interfaces 8 (2016) 2111–2119.
- [26] S. Rawalekar, T. Mokari, Adv. Energy Mater. 3 (2013) 12–27.
- [27] S. Chen, S. Shen, G. Liu, Y. Qi, F. Zhang, C. Li, Angew. Chem. Int. Ed. 54 (2015) 3047–3051.
- [28] S. Bai, J. Ge, L. Wang, M. Gong, M. Deng, Q. Kong, L. Song, J. Jiang, Q. Zhang, Y. Luo, Y. Xie, Y. Xiong, Adv. Mater. 26 (2014) 5689–5695.
- [29] P.V. Kamat, J. Phys. Chem. Lett. 3 (2012) 663–672.
- [30] Y. Lu, G.L. Liu, L.P. Lee, Nano Lett. 5 (1) (2005) 5–9.
- [31] H. Wei, X. Tian, D. Pan, L. Chen, Z. Jia, H. Xu, Nano Lett. 15 (2015) 560–564.
- [32] Y.J. Lu, J.S. Kim, H.Y. Chen, C.H. Wu, N. Dabidiani, C.E. Sanders, C.Y. Wang, M.Y. Lu, B.H. Li, X.G. Qiu, W.H. Chang, L.J. Chen, G. Shvets, C.K. Shih, S. Gwo, Science 337 (2012) 450–453.
- [33] X. Wang, J. Liu, S. Leong, X. Lin, J. Wei, B. Kong, Y. Xu, Z.X. Low, J. Yao, H. Wang, ACS Appl. Mater. Interfaces 8 (2016) 9080–9087.
- [34] R. Chandra, S. Mukhopadhyay, M. Nath, Mater. Lett. 164 (2016) 571–574.
- [35] B. Yu, F. Wang, W. Dong, J. Hou, P. Lu, J. Gong, Mater. Lett. 156 (2015) 50–53.
- [36] X. Zeng, L. Huang, C. Wang, J. Wang, J. Li, X. Luo, ACS Appl. Mater. Interfaces 8 (2016) 20274–20282.
- [37] T. Zhang, W. Lin, Chem. Soc. Rev. 43 (2014) 5982–5993.
- [38] J.L. Wang, C. Wang, W. Lin, ACS Catal. 2 (2012) 2630–2640.
- [39] T. Rodenas, I. Luz, G. Prieto, B. Seoane, H. Miro, A. Corma, F. Kapteijn, F.X. Llabrés i Xamena, J. Gascon, Nat. Mater. 14 (2015) 48–55.
- [40] X. Liu, J. Luo, Y. Zhu, Y. Yang, S. Yang, J. Alloys Compd. 648 (2015) 986–993.
- [41] L.H. Wee, N. Janssens, S.P. Sree, C. Wiktor, E. Gobechiya, R.A. Fischer, C.E. Kirschhock, J.A. Martens, Nanoscale 6 (2014) 2056–2060.
- [42] A. Balamurugan, G. Balossier, D. Laurent-Maquin, S. Pina, A.H. Rebelo, J. Faure, J.M. Ferreira, Dent. Mater. 24 (2008) 1343–1351.
- [43] J. Liu, J. He, L. Wang, R. Li, P. Chen, X. Rao, L. Deng, L. Rong, J. Lei, Sci. Rep. 6 (2016) 23667.
- [44] Z.A. Huang, Q. Sun, K. Lv, Z. Zhang, M. Li, B. Li, Appl. Catal. B 164 (2015) 420–427.
- [45] X. Jia, M. Tahir, L. Pan, Z.F. Huang, X. Zhang, L. Wang, J.J. Zou, Appl. Catal. B 198 (2016) 154–161.
- [46] W. Li, D. Li, Y. Lin, P. Wang, W. Chen, X. Fu, Y. Shao, J. Phys. Chem. C 116 (2012) 3552–3560.
- [47] F. Shi, L. Chen, M. Chen, D. Jiang, Chem. Commun. 51 (2015) 17144–17147.
- [48] P. Zhou, J. Yu, M. Jaroniec, Adv. Mater. 26 (2014) 4920–4935.
- [49] C.C. Wang, J.R. Li, X.L. Lv, Y.Q. Zhang, G. Guo, Energy Environ. Sci. 7 (2014) 2831.
- [50] C.C. Wang, X.D. Du, J. Li, X.X. Guo, P. Wang, J. Zhang, Appl. Catal. B 193 (2016) 198–216.
- [51] M.A. Nasalevich, M. van der Veen, F. Kapteijn, J. Gascon, CrystEngComm 16 (2014) 4919.